THE COMPANY OF
Biologists

Quantitative imaging of cell dynamics in mouse embryos using light-sheet microscopy

Ryan S. Udan[1],*, Victor G. Piazza[1], Chih-wei Hsu[1], Anna-Katerina Hadjantonakis[2] and Mary E. Dickinson[1],‡

ABSTRACT

Single/selective-plane illumination, or light-sheet, systems offer several advantages over other fluorescence microscopy methods for live, 3D microscopy. These systems are valuable for studying embryonic development in several animal systems, such as *Drosophila*, *C. elegans* and zebrafish. The geometry of the light path in this form of microscopy requires the sample to be accessible from multiple sides and fixed in place so that it can be rotated around a single axis. Popular methods for mounting include hanging the specimen from a pin or embedding it in 1-2% agarose. These methods can be particularly problematic for certain samples, such as post-implantation mouse embryos, that expand significantly in size and are very delicate and sensitive to mounting. To overcome the current limitations and to establish a robust strategy for long-term (24 h) time-lapse imaging of E6.5-8.5 mouse embryos with light-sheet microscopy, we developed and tested a method using hollow agarose cylinders designed to accommodate for embryonic growth, yet provide boundaries to minimize tissue drift and enable imaging in multiple orientations. Here, we report the first 24-h time-lapse sequences of post-implantation mouse embryo development with light-sheet microscopy. We demonstrate that light-sheet imaging can provide both quantitative data for tracking changes in morphogenesis and reveal new insights into mouse embryogenesis. Although we have used this approach for imaging mouse embryos, it can be extended to imaging other types of embryos as well as tissue explants.

KEY WORDS: Light-sheet, Postimplantation, Mouse embryo culture, Quantitative, Cell dynamics

INTRODUCTION

Since the invention of the light microscope, there have been continued efforts to improve resolution, contrast, speed and depth discrimination. In recent years, confocal, multiphoton, spinning disk, super-resolution and other methods have pushed these limits. Of particular interest for the study of dynamic events, there has been a strong need to image large, three-dimensional (3D) volumes with sufficiently high spatial and temporal resolution to study cellular and sub-cellular dynamics. Both confocal and multiphoton microscopy have been used in various studies to image dynamic processes within cells and tissues, but depth penetration and sensitivity can be significant limitations due to light scattering and losses associated with point scanning. Increasing laser power or dwell time can

increase fluorescent signals, but often at the expense of cell and tissue viability. To overcome these limitations, new microscopes have been designed: confocal theta microscopy (Lindek et al., 1996), selective/single-plane illumination microscopy (SPIM) (Huisken et al., 2004) and orthogonal plane fluorescence optical sectioning microscopy (Voie et al., 1993), all of which utilize a sheet of light to illuminate the sample and excite fluorescence. Light-sheet microscopes use cylindrical lens configurations (Huisken et al., 2004), digital scanning laser beams (Keller et al., 2008) or Bessel beams (Planchon et al., 2011) to create a sheet of light that is passed through the sample, resulting in a thin plane of fluorescence excitation. An objective lens is placed perpendicular or at an angle to the illumination sheet to collect the fluorescence emitted from the illumination plane (Höckendorf et al., 2012; Santi, 2011). Thus, the thin sheet provides optical sectioning to reduce the out-of-focus signal and improve resolution. Three-dimensional volumes of images can be collected by moving the sample so that the sheet crosses different *z*-depths, producing a *z*-stack, or the specimen can be rotated and imaged at successive angles to create a 3D tomogram (Huisken et al., 2004; Swoger et al., 2007). Multi-angle imaging and reconstruction can help to overcome limitations of depth penetration due to light scatter, but the ability to freely rotate the sample makes it possible to easily position and re-position the embryo without disturbing it, a distinct advantage over confocal or multiphoton microscopy. As thin image planes are detected with sensitive CCD or CMOS detectors, high-resolution, high signal-to-noise image volumes can be detected quickly with only minimal damage, making this approach ideal for live, fluorescence imaging.

There are significant advantages to imaging thick 3D specimens with light-sheet microscopy, but the imaging geometry and unique sample mount can be a limitation for imaging many specimens. Light-sheet microscopy requires that light is accessible from multiple sides, and samples are thus typically mounted in low-melting temperature agarose, fixed to a mounting pin or mounted on a pedestal. Embedding in 1-2% agarose has become popular, as it closely matches the index of refraction of water (Kaufmann et al., 2012) and specimens can be immobilized, thus facilitating the reconstruction of multi-angle datasets. Agarose embedding is ideal for mounting and imaging fixed tissues or for culturing and imaging tissues/embryos that do not exhibit significant increases in size during embryonic development (such as zebrafish, *C. elegans* and *Drosophila* embryos) (Huisken et al., 2004; Keller et al., 2008; Swoger et al., 2007; Wu et al., 2011). However, this method is impractical for imaging living samples that grow and expand in size, such as mouse embryos, and can compromise delicate tissues that are perturbed by the embedding procedure (Höckendorf et al., 2012; Lemon and Keller, 2013). Thus, there is a pressing need to develop new approaches to mount samples for light-sheet imaging.

Here, we describe a protocol for mounting post-implantation mouse embryos with intact yolk sacs for live imaging with a light-sheet microscope system. Previous work by several laboratories,

[1]Department of Molecular Physiology and Biophysics, Baylor College of Medicine, Houston, TX 77030, USA. [2]Developmental Biology Program, Memorial Sloan-Kettering Cancer Center, New York, NY 10065, USA.
*Present address: Department of Biology, Missouri State University, Springfield, MO 65897, USA.

‡Author for correspondence (mdickins@bcm.tmc.edu)

DEVELOPMENT

including our own, has shown that mouse embryos can be cultured and imaged using light microscopy at early post-implantation stages prior to the formation of the chorioallantoic placenta, thereby revealing novel dynamic events required for early development (Garcia et al., 2011a; Jones et al., 2002; Kwon et al., 2008; Pyrgaki et al., 2010; Stuckey et al., 2011; Trichas et al., 2012; Udan et al., 2013). As these embryos are very delicate and expand significantly during development, which poses serious complications for light-sheet imaging, we developed a new method for mounting mouse embryos from E6.5-8.5 for multi-angle, light-sheet microscopy to enable long-term imaging of growing embryos at a range of post-implantation stages. We show that embryos mounted for light-sheet imaging using hollow agarose cylinders can undergo robust stereotypical development. Resulting image datasets can be easily segmented, providing novel, quantitative data about cell dynamics.

RESULTS
Preparing hollow agarose cylinders to house early post-implantation mouse embryos

To create a robust growth environment for mouse embryos, we modified the agarose embedding approach to create size-appropriate, hollow agarose cylinders. We reasoned that agarose cylinders would allow delicate tissues to maintain their shape without deformation and to allow unimpeded expansion during development, while still enabling rotation for multi-angle image acquisition and 3D image reconstruction. To fit growing embryos of different developmental time points into the cylinders with minimal sample drift, agarose cylinders of various diameters were created. Small, medium and large-diameter cylinders were optimal for overnight cultures of embryonic day (E) 6.5, E7.5 and E8.5 mouse embryos, respectively, as outlined in the Materials and Methods section below.

The agarose cylinders were generated using common materials, thus making this methodology widely accessible and reproducible. To create large cylinders, a 1 ml syringe (or a small glass capillary) was filled with liquid agarose (1-2%). Immediately after filling, the end of a cotton swab (or a smaller glass capillary) was placed in the center of the agarose-filled syringe (Fig. 1A). After the agarose solidified, it was removed using a plunger. The agarose cylinders

were then cut to the desired length, removed from the cotton swab end and placed in a Petri dish with sterile PBS to prevent them from drying out (Fig. 1B). Dissected and cultured embryos were loaded into the agarose cylinders (which were placed horizontally and immersed in culture medium) by moving the embryo with dissection forceps into the open end of the cylinder. As the cylinder was raised to a vertical position, the embryo fell to the bottom of the hollow chamber (Fig. 1C-E). This allowed the embryo to be inserted into the cylinder while still remaining in the culture medium. Subsequently, the end of the cotton swab used as the initial mold was gently reinserted into the open end of the hollow chamber. The swab fitted snugly, thereby providing a means to handle the cylinder and suspend the embryo within the cylinder for imaging (Fig. 1F). Once sealed by the end of the cotton swab, culture medium was maintained within the cylinder for several minutes, keeping the embryos hydrated. However, over time, the agarose tubes were susceptible to drying out, and embryo viability was compromised by low temperatures and unsuitable pH; thus, we found it best to immediately immerse the cylinders into dissection medium in the incubator (Fig. 2A,B). Therefore, more expensive culture medium with high serum content could be used in minimal volumes inside the cylinder, while maintaining proper hydration and gas exchange with dissection medium outside the cylinder. As a twofold change in size was typically observed in E6.5-8.5 embryos over 24 h, embryos at different stages (sizes) were matched with different diameter cylinders to minimize embryo drift, while at the same time allowing sufficient space for tissue growth and expansion during the culture period.

Growing post-implantation mouse embryos in agarose cylinders

To assess the feasibility of culturing E8.5 mouse embryos in hollow agarose cylinders, embryos were grown for 24 h and the health and development were compared between embryos grown in agarose cylinders and those grown under standard *ex utero* conditions in a Petri dish. To compare conditions, a rubric was established based on the extent of blood flow and the remodeling of yolk sac vessels, similar to those used by Lucitti et al. (2007), as these parameters are more stringent descriptors of embryonic
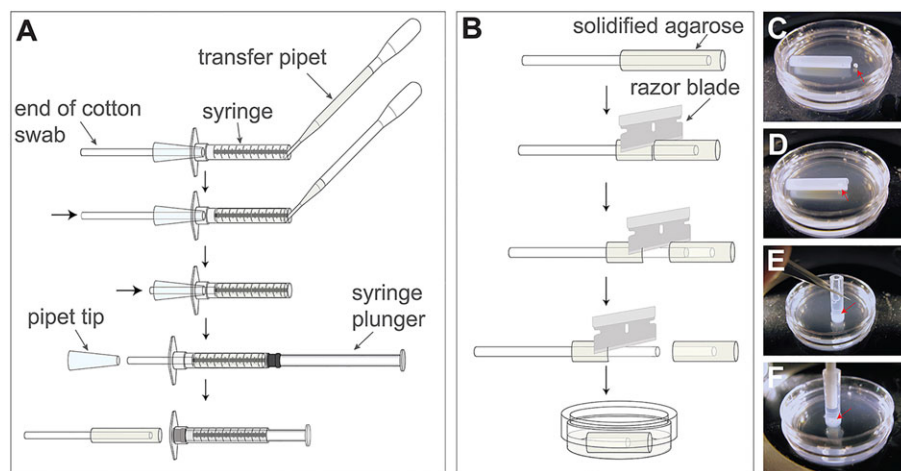

Fig. 1. Preparing hollow agarose cylinders for light-sheet microscopy of live mouse embryos. (A) A 1 ml syringe and the end of a cotton swab were used to create hollow agarose cylinders by filling the syringe with 1-2% liquid agarose, inserting the end of the swab into the middle of the syringe and extruding the solidified agarose using the syringe plunger. The cut end of a 1 ml micropipette tip was used to center the swab. (B) The hollow agarose cylinder was removed from the cotton swab stick using a razor blade and placed into a Petri dish with sterile PBS. (C-E) Live mouse embryos (red arrows) were transferred into hollow agarose cylinders (equilibrated in warm culture medium) using forceps. Embryos sink to the bottom of the agarose cylinder when the cylinder is tilted upright. (F) The cotton swab is gently reinserted into the open end of the cylinder, fitting snugly, to provide a way to handle the cylinders and mount them in the light-sheet system.
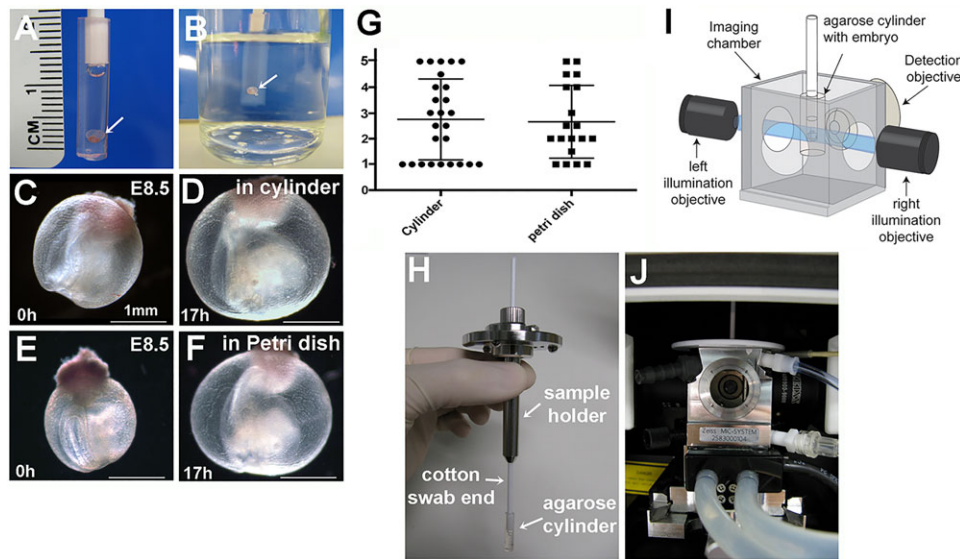
Fig. 2. Culturing mouse embryos in hollow agarose cylinders. (A) Embryos (white arrow) were cultured in hollow agarose cylinders filled with culture medium. (B) The agarose cylinder is then submerged in dissection medium. (C-F) E8.5 embryos grown in both agarose cylinders submerged in dissection medium and in a Petri dish in culture medium grew well and underwent partial to full vascular remodeling and embryo turning. Scale bars: 1 mm. (G) Comparison of static embryo culture in a Petri dish versus embryo culture in cylinders showed no significant difference in embryonic growth when judged by a five-point scale as defined in the Materials and Methods. (H) The swab and the agarose cylinder assembled in the sample holder of the Lightsheet Z.1 microscope. (I) Schematic for the light path, the agarose cylinder and the imaging chamber. (J) The stainless steel imaging chamber within the Lightsheet Z.1 microscope with the sample in place.

health than the heartbeat alone. Embryos were evaluated on a scale of 1 to 5. Embryos at 1.0 exhibited no blood flow and collapsed vessels; 2.0: no blood flow and space-filled/unremodeled vessels; 3.0: weak blood flow and unremodeled vessels; 4.0: apparent blood flow and partially remodeled vessels; 5.0: apparent blood flow and fully remodeled vessels. Embryos grown in the cylinders were comparable to those grown in Petri dishes, as embryos were able to grow, undergo embryonic turning and exhibited blood vessel remodeling (Fig. 2C-F). Statistical tests revealed that embryos grown in either the cylinder or Petri dish groups were not significantly different (χ^2=0.076, α=0.05, d.f.=2) and the average extent of remodeling was ∼2.65-2.75 (Fig. 2G). These data clearly indicate that the hollow cylinder method did not place any physical constraints on the embryos which would impair growth, and that this method is comparable to the culture methods previously established for live imaging.

Imaging-chamber setup for live embryo imaging

Although light-sheet or SPIM can be custom built, we used a commercially available system (Lightsheet Z.1, Carl Zeiss). Samples were suspended in a liquid-filled imaging chamber constructed of stainless steel and comprising four windows (Fig. 2I). Two viewing windows allowed access of the sheet of light through glass slides into the chamber, using two illumination objectives on opposite sides of the specimen. The fluorescence imaging objective was oriented at 90° from the illumination objectives. The Lightsheet Z.1 has a wide-field viewing camera opposite the detection objective that was used for sample orientation. For this study, samples were imaged with a 20×, NA 1.0 Plan-Apochromat water immersion objective (Carl Zeiss) inserted through the chamber window and sealed with a gasket.

For each overnight culture, the imaging chamber was prepared by sonication, subsequent washes with ethanol and followed by sterile PBS. The chamber was then assembled, inserted into the microscope chamber, filled with dissection medium and allowed to equilibrate with the environment for at least 10 min before the cylinder containing the embryo was lowered into the chamber center (Fig. 2H-J). The embryo was aligned with the focal plane within the light-sheet to enable optical sectioning with optimal resolution.

Light-sheet imaging of E8.5 post-implantation mouse embryos

To test the new hollow agarose cylinders in the light-sheet microscope, we imaged *Flk1-myr::mCherry*; *Flk1-H2B::eYFP* double-transgenic embryos (Fraser et al., 2005; Larina et al., 2009; Poché et al., 2009), in which endothelial cell (EC) membranes and nuclei were labeled with mCherry and yellow fluorescent protein (YFP), respectively, similar to our previous studies (Udan et al., 2013). For embryos between E8.5 and E9.5, we used agarose cylinders with a 4.7 mm outer diameter and a 2.5 mm inner diameter (see Materials and Methods). We observed a very bright and robust signal in both the YFP and mCherry channels, and throughout the 24-h culture period there was vigorous blood flow and continuous growth of the embryo. Whereas in previous studies we had focused on particular regions of the embryo for imaging and analysis related to vessel remodeling (Udan et al., 2013), the ability to rotate the embryo position easily allowed us to acquire data from multiple regions of a particular embryo, revealing new information about embryonic development. We focused on the region of the yolk sac adjacent to the ventral part of the embryo. This region of the yolk sac is avascular during early somite stages and shows dynamic movement as the yolk sac shifts and closes during embryo turning (supplementary material Movie 1). As the summary images show, we identified specific groups of ECs that migrate during yolk sac closure, as well as EC sprouting events from the vascularized part of the yolk sac into the avascular area (supplementary material Movie 1; Fig. 3A,B, arrows). Using image segmentation and cell tracking, we examined changes in the avascular spaces within the plexus over time and found that although there was consistent movement forward as the yolk sac shifted during closure (Fig. 3A-D, blue arrows), the sizes and relative positions of the avascular spaces to each other were largely unchanged (Fig. 3C,D). However, tracking individual nuclei revealed distinct regions of EC motility. Near the yolk sac/embryo border, we identified a group of cells that were actively migrating forward in long, straight trajectories (Fig. 3E,F, white arrows), but ECs behind this front were distinct, showing very little forward migration (short, random trajectories) (Fig. 3E,F, white arrows). These trajectories are overlaid on both the 4.7 h image (E) and the 14.5 h image (F) to show the position of the cell nuclei at the beginning and end of the
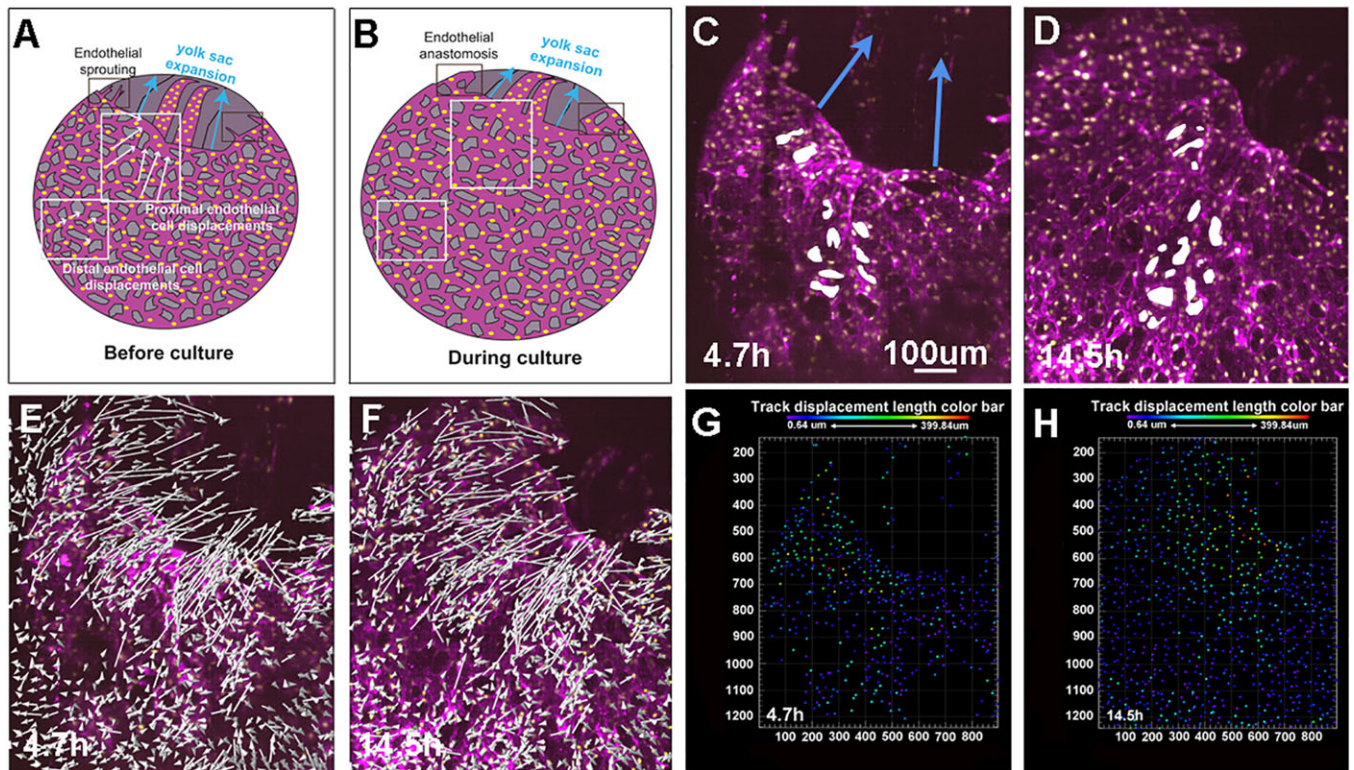
Fig. 3. Live imaging of *Flk1-myr::mCherry*- and *Flk1-H2B::eYFP*-labeled endothelial cells revealed endothelial cell migrations at the border of the vascular and avascular space. (A,B) Depiction of entire E8.5 embryo showing four key events captured during the time lapse: yolk sac expansion (blue arrows), two regions of EC migrations, proximal to the edge of the yolk as well as distal from the edge (white arrows and white boxes), and sprouting angiogenesis/vessel anastomosis (brown box) at the edge of the yolk sac. (C,D) Select images from time-lapse sequences (4.7 h and 14.5 h) showing EC nuclei (YFP) and membrane (mCherry fluorescent protein) of cultured E8.5 embryo and yolk sac. During the culture, yolk sac and blood vessel expansion occurs around the embryos, as indicated by the blue arrows in C and the final position of the yolk sac, while the avascular spaces are maintained (selected white shapes). (E,F) Endothelial cells close to the edge of the yolk sac show directed migration trajectories as it begins to close (white arrows). E, the same image shown as in C, overlaid with the final migration trajectories to indicate the state of the tissue at 4.7 h. F similarly shows the 14.5 h image as in D, overlaid with the final trajectories. (G,H) Colored maps indicate ECs at 4.7 h (G) and 14.5 h (H) with large displacement lengths (>200 μm, green, yellow and red spheres in G,H). In the region more distal from the edge, ECs showed smaller displacement lengths (<100 μm, blue spheres in G,H). Images were acquired with a 20×, NA=1.0 objective, zoom=0.4, every 10 min for 16.5 h, *z*-step=2.67 μm, total *z*-depth=411.18 μm. Scale bar in C: 100 μm.

elapsed period. To discern this pattern more easily, we created a map of migration distance for each cell nucleus that was tracked (Fig. 3G,H), showing the starting position (Fig. 3G) and end position of the nuclei (Fig. 3H). The rainbow color indicator shows much longer migration lengths (green-yellow-orange nuclei) clustered toward the edge of the yolk sac compared with those behind this front (blue-purple nuclei). Thus, there appeared to be differential EC migration activity at the edge that might play a role in yolk sac closure.

Moving to a different region of the vascular/avascular border, we found numerous individual vessel sprouting events (supplementary material Movie 2; Fig. 4A-D). Vessel sprouting had not been observed in our previous analysis of these reporter mice during vessel remodeling. This was due to the difficulty in imaging this region of the embryo on a confocal microscope, as the ectoplacental cone causes the embryo to lie on its side. However, the ease of positioning the imaging angle on the light-sheet enabled us to see clearly that there were numerous sprouts from the plexus into the avascular region. Interestingly, as development proceeded, these sprouts fused and anastomosed (Fig. 4D).

The ability to freely position the embryo also made it possible to visualize the fusion of the dorsal aortae (supplementary material Movie 3; Fig. 3E-H). We were previously unable to capture this process using the inverted confocal microscope, as embryos lie on

their sides and it is difficult to position them without deleterious consequences to the blood flow. The light-sheet system offers the significant advantage of being able to position the embryo freely along the *x*-, *y*- and *z*-planes, and in rotating the sample. Although dorsal aorta fusion in avian embryos is thought to occur progressively from anterior to posterior (Garriock et al., 2010), the mouse embryo data revealed two different places where the dorsal aorta approximates (Fig. 4E-H, white arrows), rather than a continuous unidirectional, zipper-like fusion.

Light-sheet imaging of gastrulating mouse embryos
We next adapted the hollow cylinder design to image earlier embryos at E6.5. Previous studies have imaged gastrulating embryos using light-sheet microscopy with a horizontal mounting procedure, imaging the embryo from the distal end (Ichikawa et al., 2013). For E6.5 embryos, we used a glass capillary instead of the 1 ml syringe to create agarose cylinders with a small outer diameter (1.5 mm) and a piston rod to make the cylinder hollow (see Materials and Methods). A medium-sized chamber was also made for the dimensions of E7.5 embryos and is described in the Materials and Methods. To test the E6.5 cylinders, we used *TCF/Lef-H2B::eGFP* transgenic embryos to visualize cells that have activated the canonical Wnt signaling pathway during gastrulation. This reporter has been shown to label part of the visceral endoderm, as well as the
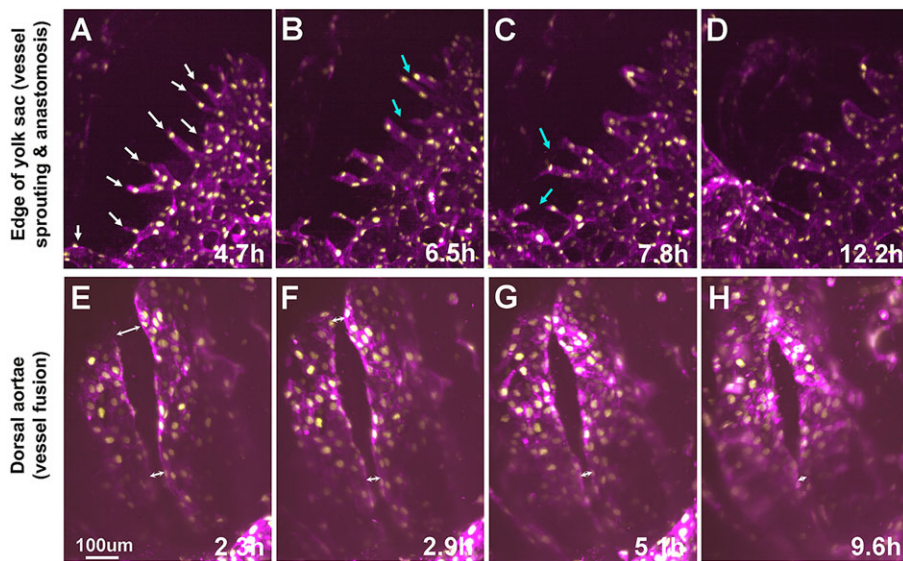
Fig. 4. Analysis of dynamic events within the yolk sac and embryo. (A-D) Time-lapse images of E8.5 yolk sacs revealed sprouting angiogenesis (A, white arrows) at the edge of the yolk sac, followed by vessel anastomosis (B-C, blue arrows). Images were acquired with a 20×, NA=1.0 objective, zoom=0.4, every 10 min for 7.5 h, z-step=2.67 μm, total z-depth=411.18 μm. (E-H) Time-lapse, light-sheet microscopy images of paired dorsal aorta fusion (double arrows) showing that the opposing aorta are coming together at two different regions, but not progressively from a single starting point. Images were acquired with 20× Objective, NA=1.0, zoom=0.4, every 8 min for 7 h 36 m, z-step size=1.484 μm, total z-depth=71.22 μm. Scale bar: 100 μm.

primitive streak and nascent mesoderm in gastrulating embryos at E6.5 (Ferrer-Vaquer et al., 2010).

Mounting the embryos within a hollow agarose cylinder enabled multi-angle imaging of these embryos, and a full 3D reconstruction is shown in Fig. 5. Light scatter did not permit images to be collected through the entire embryo from a single angle (Fig. 5A-C), but the entire 3D volume of an E6.5 embryo could be reconstructed from z-stacks acquired at five different angles (supplementary material Movies 4,5; Fig. 5D-I). The use of the agarose walls of the cylinder enabled the embedding of fluorescent beads to aid in reconstruction while the inner chamber accommodated embryo growth.
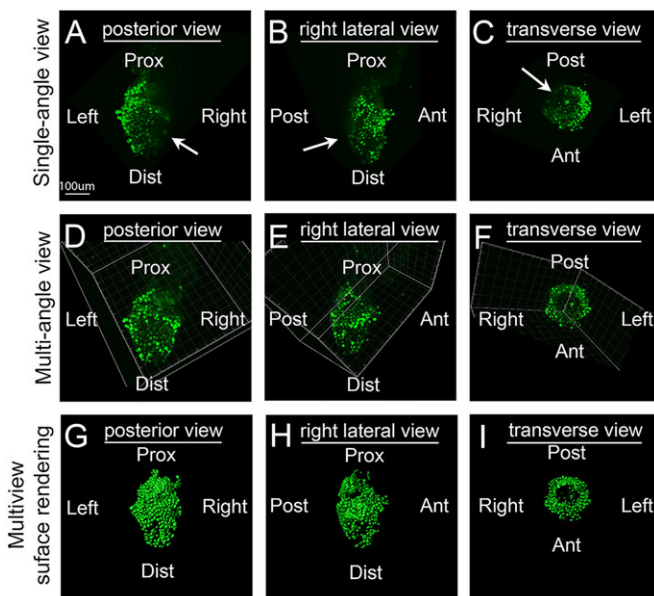

Fig. 5. Single- and multi-angle 3D reconstructions of an E6.5 TCF/LEF-H2B::eGFP mouse embryo. (A-I) 3D transparency projections of a TCF/LEF-H2B::eGFP-labeled E6.5 mouse embryo, posterior view (A,D,G), right lateral view (B,E,H) or transverse view (C,F,I). (A-C) 3D projections taken from a single-angle revealed attenuation of the fluorescence signal (arrows). (D-F) Deeper signals within the embryo were recovered using multi-angle imaging as shown in the 3D transparency projections. (G-I) Surface rendering of the multi-angle images (D-F) revealed the 3D volume of the embryo. Scale bar: 100 μm.

Over the 24-h period of time-lapse imaging, the cylinders provided sufficient space to allow for unimpeded twofold expansion of the embryo. Images of live E6.5 embryos with the light-sheet system revealed many brightly fluorescent cells undergoing division and moving anteriorly within the embryo (supplementary material Movie 6; Fig. 6). For further analysis of cell movements in these embryos, we analyzed 572 z-sections representing images taken through half of the embryo from one angle, and GFP+ cells were tracked in 3D using Imaris software. We observed both GFP+ endoderm cells near the surface of the embryo and deeper GFP+ cells within the mesoderm (~50-70 μm below the surface). Fig. 6A-F and supplementary material Movie 6 show the 3D migration tracks for selected cells indicated by colored dragon tail tracks. The 24-h movie is broken down into six panels, each from a selected time point (Fig. 6A, 5 h 30 min; B, 8 h 50 min; C, 12 h 10 min; D, 15 h 30 min; E, 18 h 50 min; F, 22 h 10 min), but each track shown in the panel was plotted from 2.5 h of data prior to the time point. At earlier time points, we detected more limited movements of bright, GFP+ endoderm nuclei moving radially away from the center of the image, correlating with the growth of the embryo (Fig. 6A-C). However, once gastrulation began, we detected longer tracks of gastrulating mesodermal cells. By 15.5 h, the density of GFP+ cells in the posterior (right of image) increased and we detected several cells migrating anterolaterally over large distances (Fig. 6E,F). Several mitotic events were also detected in the imaging data and cell division was observed both in non-migrating as well as actively migrating cells (supplementary material Movie 6, and data not shown). These data demonstrate the wealth of quantitative data that can be obtained from simultaneous cell movements in different regions of the developing embryo during gastrulation.

DISCUSSION
Here, we have demonstrated the use of hollow agarose cylinders filled with culture medium for robust, reproducible and successful imaging of early post-implantation mouse embryos. This technique uses light-sheet microscopy for periods of up to 24 h and allows for multi-angle acquisition. A previous report had shown that E5.5 mouse embryos could be mounted horizontally to an acrylic rod for light-sheet imaging, revealing extensive dynamics of cell nuclei in the early gastrula (Ichikawa et al., 2013). Embryos were held in place by the tension of the extra-
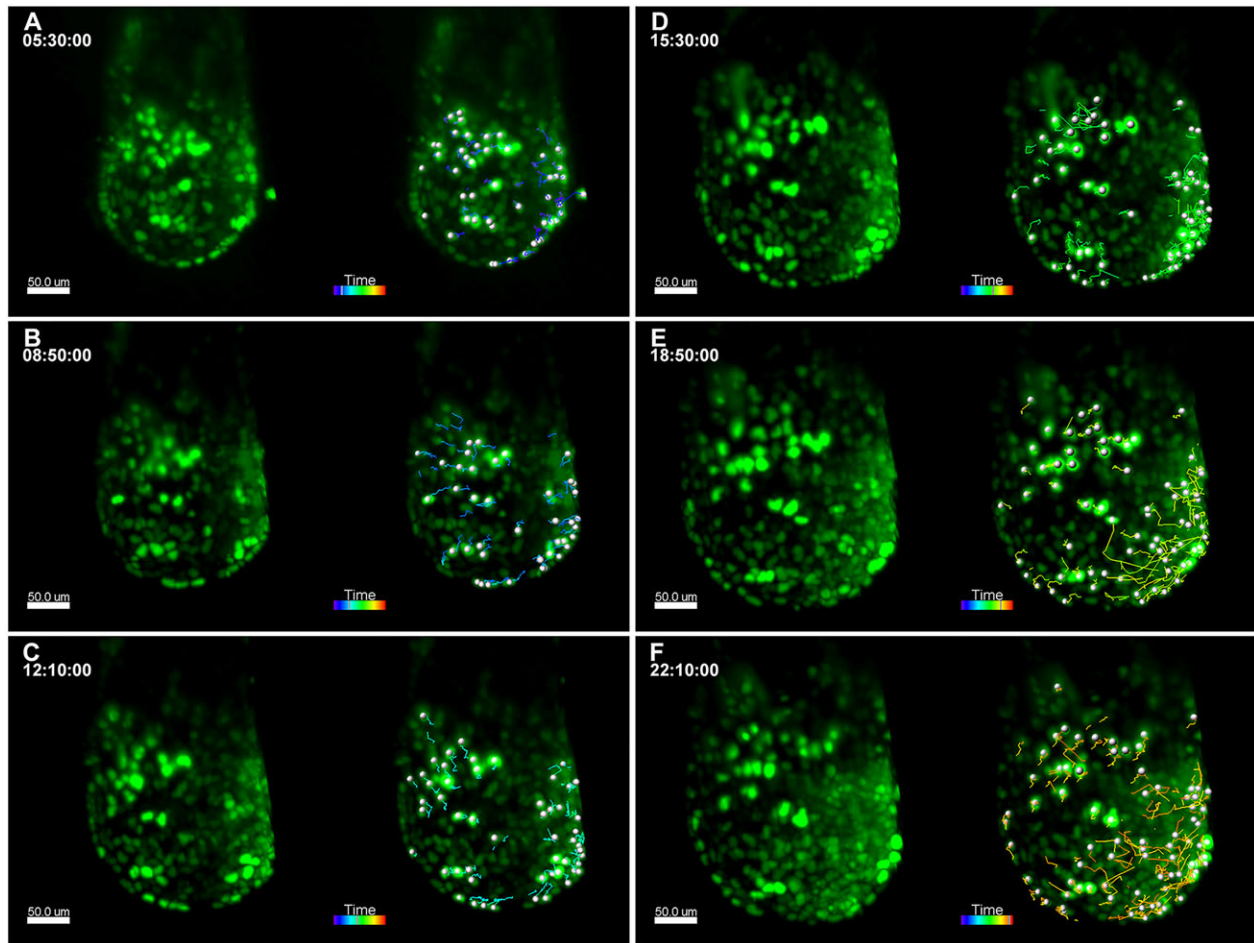
DEVELOPMENT

Fig. 6. Live imaging of *TCF/LEF-H2B::eGFP* E6.5 embryos using agarose cylinders and 3D tracking of endothelial cells. For all panels, images from select time points from the 3D time-lapse movie are on the left and images from the movie overlaid with Imaris 3D tracking data are on the right. Embryos are oriented with the anterior side on the left. (A-F) Cultured embryos in hollow agarose cylinders show a twofold increase in embryo size over 24 h. Images from select time points are shown (A, 5 h 30 min; B, 8 h 50 min; C, 12 h 10 min; D, 15 h 30 min; E, 18 h 50 min; F, 22 h 10 min), and 3D cell tracks represent cell movements that occurred during the 2.5-h time period before the respective time point. Images from early time points show passive, radial cell movements associated with embryo growth (A-C), while images from later time points (E-F) show distinct antero-lateral migration events of deeper *TCF/LEF-H2B::eGFP*^{+} cells as gastrulation begins. GFP^{+} endoderm cells on the surface show less movement. Images were taken with a 20× objective, NA=1.0, zoom=0.7, every 10 min for a total of 24 h, *z*-step size=1.14 μm, total *z*-depth=115 μm. Scale bars: 50 μm.

embryonic tissue inserted into a hole in a plastic rod. Although reported to be stable for the 3-10 h of imaging (Ichikawa et al., 2013), we found that, as embryos grew, particularly for >8 h, they often became dislodged or distorted. Moreover, by keeping the embryo in a fixed position, with the proximal-distal axis aligned to the optical axis of the lens, there was no way to rotate the embryo, taking away a key advantage of the light-sheet system. For most light-sheet systems, including the commercially available Lightsheet Z.1, automated rotation is designed to rotate a sample that is mounted vertically and perpendicular to the optical axis of the collection objective. Thus, we aimed to develop a method that could be used for long periods (at least 24 h), that would preserve the ability to freely rotate the sample 360° to acquire multi-angle images or simply allow for ease of positioning for single-angle imaging, and that could be used for a range of early post-implantation stages. The new approach we have developed here using agarose cylinders accomplishes these goals and allows for normal development of mouse embryos at E6.5-8.5 for up to 24 h.

We believe that the success of this approach can be attributed to a number of parameters. First, the space within the cylinder allows for significant expansion of the embryo as it develops normally, but

limits movement sufficiently to stabilize the sample during imaging. For instance, we observed a twofold expansion in embryo size over 24 h in E6.5 *TCF/Lef-H2B::eGFP* embryos; hence, the inner diameter of the cylinder was optimized to allow expansion but minimize movement and drift. Second, the embryos are continuously immersed in medium throughout the mounting and imaging procedure, thereby reducing the chance of damaging delicate embryos. Third, the inside of the agarose cylinder can be filled with small volumes of embryo culture medium, but by immersing the cylinder in dissection medium, gas and medium exchange with the larger reservoir within the imaging chamber is permitted. Eventually, higher concentrations of serum in the culture medium will probably equilibrate with those in the dissection medium via diffusion. This might impact attempts to lengthen the imaging time significantly, but this has not yet been tested empirically. Finally, the cylinders can be rotated and imaged from any direction to capture data from many angles, without additional perturbation of the embryo. Although other researchers have used hollow plastic tubing with a similar refractive index to water (such as fluorinated ethylene propylene, FEP) (Kaufmann et al., 2012), or small chambers comprising thin Teflon-based

DEVELOPMENT

transparent walls (Keller et al., 2007) to house zebrafish embryos, the agarose chambers have the advantage that they can be easily customized to match the inner diameter to the size of the sample. In addition, agarose permits diffusion of gas and medium, thus making the agarose chambers superior for application to mouse embryos. Although we used this method to image mouse embryos, this methodology could be readily adapted to imaging a wide variety of growing embryo types and tissue explants with light-sheet microscopy. By providing an open space for specimens to expand, hollow agarose cylinders represent a more effective and less restrictive mounting format than embedding specimens in solid agarose.

As others have shown (Höckendorf et al., 2012; Huisken et al., 2004; Keller, 2013), we observed significant gains in tissue viability and image resolution compared with confocal microscopy imaging. Light-sheet illumination reduces the exposure of the out-of-focus regions to excitation light, thereby minimizing photobleaching and photodamage. We noticed a distinct improvement in the retention of fluorescent protein signal compared with previous studies of *Flk1-myr::mCherry*; *Flk1-H2B::eYFP*-labeled endothelial cells using confocal microscopy (Udan et al., 2013). Moreover, the improvement in fluorescence stability did not require sacrificing the signal-to-noise ratio, two-dimensional (2D) field-of-view or 3D volume as we have observed for conventional confocal microscopy. This allowed us to capture larger image volumes and extract more data from each movie. The high resolution, high signal-to-noise time-series images provided data that could be easily processed using software such as Imaris to track the movements of individual cells (Fig. 3E-H, Fig. 6A-F) and to segment features such as the avascular spaces present between growing vessels (Fig. 3A-D). A similar advantage was noted for earlier embryos, in which we were able to track the movements of hundreds of migrating cells during gastrulation and embryo expansion (Fig. 6).

Using the methods reported here revealed new information about early mouse development. The new hollow agarose cylinders enabled multi-angle imaging, which is not only an advantage when collecting information from a complete volume of tissue (supplementary material Movies 4,5; Fig. 5), but also provided considerably more freedom to choose an angle of imaging than in confocal microscopy. This advantage allowed us to view for the first time events related to yolk sac closure and dorsal aorta fusion, which are difficult to capture in a system where gravity often dictates how the embryo aligns with the optical axis. First, we noted a region of endothelial cells near the edge of the vascularized part of the yolk sac that exhibit greater migratory behavior than their neighbors. We also observed a significant number of new vessels sprouting and of anastomosis events at this border. It is interesting to speculate that these movements might play a role in yolk sac closure or perhaps even turning. It is possible that EC migration and vessel sprouting could be triggered in response to changes in the expression of repulsive molecules that initially establish the avascular regions (Meadows et al., 2012). Finally, whereas we had initially assumed that dorsal aorta closure occurred in a zipper-like, anterior-to-posterior fashion as in avian embryos (Garriock et al., 2010), we observed, by contrast, closure occurring from both the anterior and posterior side. Perhaps this is related to differences in embryo posture between mammalian and avian embryos (flat versus curved). This could alter tissue tension or gradients of soluble factors, or suggest a distinct molecular mechanism active in mice. Live-imaging studies of neural tube closure have revealed both zipper-like and button-like mechanisms (Pyrgaki et al., 2010) and might provide insights into mechanisms underlying dorsal aorta

fusion. It will be important to use the improved imaging methods established here to further delineate the mechanisms underlying these novel observations.

As light-sheet microscopes become more widely available, so will the ability to perform more complex live image acquisition and data analysis experiments. By overcoming embryo or organ explant mounting issues, we have demonstrated the ability to grow post-implantation mouse embryos for up to 24-h time periods, to visualize diverse dynamic morphogenetic events, with greater ease of sample orientation, and to acquire clear high-resolution images with minimal sample photodamage or reporter photobleaching. Whereas this study reports improved culture methods for light-sheet microscopy, numerous laboratories have promoted the continued development of hardware to permit better depth penetration (Truong et al., 2011) or shallow angle imaging for specimens such as *C. elegans* (Cutrale and Gratton, 2012; Wu et al., 2011). Development of new hardware, in parallel with improved sample mounting and culture techniques, is paramount for the dissemination of this technology, and for expanding the number of applications and open questions that could be addressed using light-sheet microscopic imaging.

MATERIALS AND METHODS
Creating agarose cylinders
Sterile conditions were used for preparation of agarose cylinders, with all preparations performed in a tissue culture hood. Different materials were used to mold agarose cylinders of different sizes (small, medium or large). For large cylinders (accommodating E8.5-9.5 mouse embryos), a standard 1 ml syringe was used, with its tip cut off at the front end and the plunger removed. A 1 ml pipette tip was cut off at the end and placed at the end of the syringe to balance the end of a cotton swab [Puritan Medical Products, catalog number 25-806 1PR (plastic handle)]. Subsequently, the end of the cotton swab was inserted through the pipette tip and into the syringe interior to create a hollow cylinder. A sterile transfer pipette was used to fill the front end of the syringe with 1.5-2% liquid agarose (Ameresco, 232-731-8; microwave-heated until boiling), and the cotton swab was pushed into the interior of the syringe, but with sufficient space left at the front end of the syringe to create the bottom of the agarose cylinder. After ~5 min, the pipette tip was removed and the plunger was used to remove the now solidified agarose cylinder and cotton swab. Excess agarose was removed with a razor blade, and the agarose was pushed off the cotton swab and placed in a Petri dish filled with sterile PBS. The external diameter of the cylinder was ~4.7 mm, the internal diameter was 2.5 mm and the length of the cylinder was 20 mm.

For small- (E6.5-7.5) and medium-sized agarose cylinders- (E7.5-8.5), glass capillaries were used instead of 1 ml syringes. For small cylinders, a 50 µl glass capillary (Brand, 701908) was used to create an agarose cylinder with an external diameter of 1.5 mm. A piston rod for a transferpettor (Brand, 701936) was centered by hand to make a hollow chamber of 600 µm. For medium cylinders, a 200 µl glass capillary (Brand, 701910) was used to form an agarose cylinder with an external diameter of 2.15 mm, and a 10 µl glass capillary (Brand, 701902) was used to create a hollow 1.2 mm diameter space (Note that the internal capillary of the 10 µl glass capillary used was previously filled with agarose to create a solid tube). The cylinders were removed from the capillary using a plunger.

Dissecting and culturing post-implantation mouse embryos in agarose cylinders
Embryos were dissected in dissection medium (DMEM/F12, 10% FBS, 1× penicillin/streptomycin) as described previously (Garcia et al., 2011a,b,c; Udan and Dickinson, 2010), but using DMEM/F12 instead without the Phenol Red indicator dye [DMEM/F12 (Invitrogen, 11039-021)]. Embryos were allowed to recover in dissection medium in an incubator (37°C, 5% CO_2, 95% air) for 1 h after dissection. During the recovery period, agarose cylinders were equilibrated in culture medium [5:1 dissection medium:rat

serum (prepared in our lab, see Udan and Dickinson, 2010)] for 1 h in the incubator. After recovery, embryos were transferred to the Petri dish with the culture medium and the agarose cylinders (lying flat in culture medium). Embryos were gently moved inside the opening of the hollow cylinder. Using forceps, the cylinder was then moved vertically and the embryo was allowed to drop to the bottom of the cylinder filled with culture medium (Fig. 1E). The embryo and hollow cylinder were attached to the end of the cotton swab (or end of the glass capillary) by gently reinserting the swab into the open end of the cylinder, placed in a bottle of dissection medium, and were allowed to recover in the incubator for 1 h. For controls, embryos grown in the Petri dish were moved to a dish containing culture medium. Procedures for E6.5 embryos were similar to those described above except that a mix of 5% CO_2, 5% O_2 and balanced N_2 was used during the culture period.

Light-sheet imaging chamber setup

For live imaging, the disassembled stainless steel chamber of the light-sheet microscope was rinsed with distilled water and with 70% ethanol. It was then immersed in distilled and Milli-Q-purified water in an aquasonic sonicator (VWR, 50HT), and sonicated for 35 min at 80°C, as per the manufacturer's instructions. After cooling and drying, the chamber was reassembled with glass coverslips inserted into the illumination windows, held in place with rubber O-rings and the metal locking ring. The chamber was checked for leaks by plugging the objective window with a 5 ml centrifuge tube and filling the chamber with 70% ethanol. When leaks were detected, the chamber was disassembled and the assembly was repeated. The assembled chamber was then attached to the Peltier unit (which maintains the temperature) and its metal base. The temperature sensor was connected and fluid and gas supplies were attached by a Luer lock. The entire assembled chamber was inserted into the light-sheet and a 20×, NA1.0 Plan-Apochromat water immersion objective (Carl Zeiss) sealed the chamber from the imaging side. A white piece of plastic, washed with ethanol, was placed atop the chamber to enclose it. The chamber was filled with dissection medium, using the bottom Luer lock and a 50 ml syringe, and the Peltier unit was activated and set at 37°C. To control the humidified air intake, tubing from a top port was connected to a bubbler (at 37°C) receiving air from a CO_2 regulator. For E6.5 embryos, a mix of 5% CO_2, 5% O_2 and balanced N_2 was used. For E8.5 embryos, a mix of 5% CO_2 and 95% air was used. The embryo in the cylinder, attached to the cotton swab/piston end, was then attached to a sample holder (Fig. 2H) and inserted into the top of the light-sheet. The plastic lid at the top of the chamber was temporarily removed and the specimen was then lowered, using the stage control functions, into the interior of the chamber, with the camera used to visualize the orientation/position of the sample.

Imaging parameters

For all images, a 20×, NA1.0 Plan-Apochromat water immersion objective (Carl Zeiss) and dual-sided illumination were used. Laser power and exposure times varied depending on the amount of fluorescent signal and proximity of the signal to the surface of the tissue. For *Flk1-myr::mCherry* and *Flk1-H2B::eYFP* imaging we used 2.6% (488 nm laser) and 5.5% (561 nm laser) laser power and a 20 ms exposure time. For *TCF/Lef-H2B::eGFP* imaging, we used 3% (488 nm laser) laser power and a 49.9 ms exposure time. Other imaging parameters (alignment, zoom, pixel dimension, laser power, exposure time, z-slices and time lapses) were optimized in a similar manner to standard confocal microscopy. For all 3D datasets, a z-interval of 1-3 μm was used and 2048×2048 pixel, 16-bit images were collected. For time-lapse sequences, 66-200 z-slices were acquired for up to100 time points, resulting in datasets ranging from 87 to 264 Gigabytes (Gb).

For 2D cell tracking, Zeiss ZEN software was used to create a maximum intensity projection. For 3D cell tracking, due the large file sizes generated, images were converted to one-channel, 8-bit TIF files, and 'spot' analysis was used in Imaris software (Bitplane) for cell tracking.

For 3D image reconstructions, the multi-view acquisition feature in ZEN was used to acquire an entire z-stack from five equidistant angles (0°, 72°, 144°, 216° and 288°). 3D images were reconstructed with ZEN software. Small fluorescent beads (1 μm; Sigma, L2778) were embedded in 2% agarose cylinders (dilution 1:100,000) and were used as fiducial markers to aid in the reconstruction.

Author contributions
R.S.U. designed and performed the experiments, and wrote and edited the manuscript. V.G.P. assisted with the experiments and edited the manuscript. C.-W.H. assisted with 3D reconstructions, figure development and edited the manuscript. A.-K.H. contributed the *TCF-LEF-H2B::GFP* mouse line and edited the manuscript. M.E.D. designed the experiments, wrote and edited the manuscript.

References

Cutrale, F. and Gratton, E. (2012). Inclined selective plane illumination microscopy adaptor for conventional microscopes. *Microsc. Res. Tech.* **75**, 1461-1466.

Ferrer-Vaquer, A., Piliszek, A., Tian, G., Aho, R. J., Dufort, D. and Hadjantonakis, A.-K. (2010). A sensitive and bright single-cell resolution live imaging reporter of Wnt/ss-catenin signaling in the mouse. *BMC Dev. Biol.* **10**, 121.

Fraser, S. T., Hadjantonakis, A.-K., Sahr, K. E., Willey, S., Kelly, O. G., Jones, E. A. V., Dickinson, M. E. and Baron, M. H. (2005). Using a histone yellow fluorescent protein fusion for tagging and tracking endothelial cells in ES cells and mice. *Genesis* **42**, 162-171.

Garcia, M. D., Udan, R. S., Hadjantonakis, A. K. and Dickinson, M. E. (2011a). Live imaging of mouse embryos. *Cold Spring Harb. Protoc.* **2011**, ppdb top104.

Garcia, M. D., Udan, R. S., Hadjantonakis, A. K. and Dickinson, M. E. (2011b). Preparation of postimplantation mouse embryos for imaging. *Cold Spring Harb. Protoc.* **2011**, ppdb prot5594.

Garcia, M. D., Udan, R. S., Hadjantonakis, A. K. and Dickinson, M. E. (2011c). Preparation of rat serum for culturing mouse embryos. *Cold Spring Harb. Protoc.* **2011**, ppdb prot5593.

Garriock, R. J., Czeisler, C., Ishii, Y., Navetta, A. M. and Mikawa, T. (2010). An anteroposterior wave of vascular inhibitor downregulation signals aortae fusion along the embryonic midline axis. *Development* **137**, 3697-3706.

Höckendorf, B., Thumberger, T. and Wittbrodt, J. (2012). Quantitative analysis of embryogenesis: a perspective for light sheet microscopy. *Dev. Cell* **23**, 1111-1120.

Huisken, J., Swoger, J., Del Bene, F., Wittbrodt, J. and Stelzer, E. H. K. (2004). Optical sectioning deep inside live embryos by selective plane illumination microscopy. *Science* **305**, 1007-1009.

Ichikawa, T., Nakazato, K., Keller, P. J., Kajiura-Kobayashi, H., Stelzer, E. H. K., Mochizuki, A. and Nonaka, S. (2013). Live imaging of whole mouse embryos during gastrulation: migration analyses of epiblast and mesodermal cells. *PLoS ONE* **8**, e64506.

Jones, E. A. V., Crotty, D., Kulesa, P. M., Waters, C. W., Baron, M. H., Fraser, S. E. and Dickinson, M. E. (2002). Dynamic in vivo imaging of postimplantation mammalian embryos using whole embryo culture. *Genesis* **34**, 228-235.

Kaufmann, A., Mickoleit, M., Weber, M. and Huisken, J. (2012). Multilayer mounting enables long-term imaging of zebrafish development in a light sheet microscope. *Development* **139**, 3242-3247.

Keller, P. J. (2013). Imaging morphogenesis: technological advances and biological insights. *Science* **340**, 1234168.

Keller, P. J., Pampaloni, F. and Stelzer, E. H. (2007). Three-dimensional preparation and imaging reveal intrinsic microtubule properties. *Nat. Methods* **4**, 843-846.

Keller, P. J., Schmidt, A. D., Wittbrodt, J. and Stelzer, E. H. K. (2008). Reconstruction of zebrafish early embryonic development by scanned light sheet microscopy. *Science* **322**, 1065-1069.

Kwon, G. S., Viotti, M. and Hadjantonakis, A.-K. (2008). The endoderm of the mouse embryo arises by dynamic widespread intercalation of embryonic and extraembryonic lineages. *Dev. Cell* **15**, 509-520.

Larina, I. V., Shen, W., Kelly, O. G., Hadjantonakis, A.-K., Baron, M. H. and Dickinson, M. E. (2009). A membrane associated mCherry fluorescent reporter line for studying vascular remodeling and cardiac function during murine embryonic development. *Anat. Rec.* **292**, 333-341.

Lemon, W. C. and Keller, P. J. (2013). Live imaging of nervous system development and function using light-sheet microscopy. *Mol. Reprod. Dev.*

Lindek, S., Cremer, C. and Stelzer, E. H. K. (1996). Confocal theta fluorescence microscopy with annular apertures. *Appl. Opt.* **35**, 126-130.

Lucitti, J. L., Jones, E. A. V., Huang, C., Chen, J., Fraser, S. E. and Dickinson, M. E. (2007). Vascular remodeling of the mouse yolk sac requires hemodynamic force. *Development* **134**, 3317-3326.

Meadows, S. M., Fletcher, P. J., Moran, C., Xu, K., Neufeld, G., Chauvet, S., Mann, F., Krieg, P. A. and Cleaver, O. (2012). Integration of repulsive guidance cues generates avascular zones that shape mammalian blood vessels. *Circ. Res.* **110**, 34-46.

Planchon, T. A., Gao, L., Milkie, D. E., Davidson, M. W., Galbraith, J. A., Galbraith, C. G. and Betzig, E. (2011). Rapid three-dimensional isotropic imaging of living cells using Bessel beam plane illumination. *Nat. Methods* **8**, 417-423.

Poché, R. A., Larina, I. V., Scott, M. L., Saik, J. E., West, J. L. and Dickinson, M. E. (2009). The Flk1-myr::mCherry mouse as a useful reporter to characterize multiple aspects of ocular blood vessel development and disease. *Dev. Dyn.* **238**, 2318-2326.

Pyrgaki, C., Trainor, P., Hadjantonakis, A.-K. and Niswander, L. (2010). Dynamic imaging of mammalian neural tube closure. *Dev. Biol.* **344**, 941-947.

Santi, P. A. (2011). Light sheet fluorescence microscopy: a review. *J. Histochem. Cytochem.* **59**, 129-138.

Stuckey, D. W., Clements, M., Di-Gregorio, A., Senner, C. E., Le Tissier, P., Srinivas, S. and Rodriguez, T. A. (2011). Coordination of cell proliferation and anterior-posterior axis establishment in the mouse embryo. *Development* **138**, 1521-1530.

Swoger, J., Verveer, P., Greger, K., Huisken, J. and Stelzer, E. H. K. (2007). Multi-view image fusion improves resolution in three-dimensional microscopy. *Opt. Expr.* **15**, 8029-8042.

Trichas, G., Smith, A. M., White, N., Wilkins, V., Watanabe, T., Moore, A., Joyce, B., Sugnaseelan, J., Rodriguez, T. A., Kay, D. et al. (2012). Multi-cellular rosettes in the mouse visceral endoderm facilitate the ordered migration of anterior visceral endoderm cells. *PLoS Biol.* **10**, e1001256.

Truong, T. V., Supatto, W., Koos, D. S., Choi, J. M. and Fraser, S. E. (2011). Deep and fast live imaging with two-photon scanned light-sheet microscopy. *Nat. Methods* **8**, 757-760.

Udan, R. S. and Dickinson, M. E. (2010). Imaging mouse embryonic development. *Methods Enzymol.* **476**, 329-349.

Udan, R. S., Vadakkan, T. J. and Dickinson, M. E. (2013). Dynamic responses of endothelial cells to changes in blood flow during vascular remodeling of the mouse yolk sac. *Development* **140**, 4041-4050.

Voie, A. H., Burns, D. H. and Spelman, F. A. (1993). Orthogonal-plane fluorescence optical sectioning: three-dimensional imaging of macroscopic biological specimens. *J. Microsc.* **170**, 229-236.

Wu, Y., Ghitani, A., Christensen, R., Santella, A., Du, Z., Rondeau, G., Bao, Z., Colon-Ramos, D. and Shroff, H. (2011). Inverted selective plane illumination microscopy (iSPIM) enables coupled cell identity lineaging and neurodevelopmental imaging in Caenorhabditis elegans. *Proc. Natl. Acad. Sci. USA* **108**, 17708-17713.

DEVELOPMENT

Supplementary Movie legends
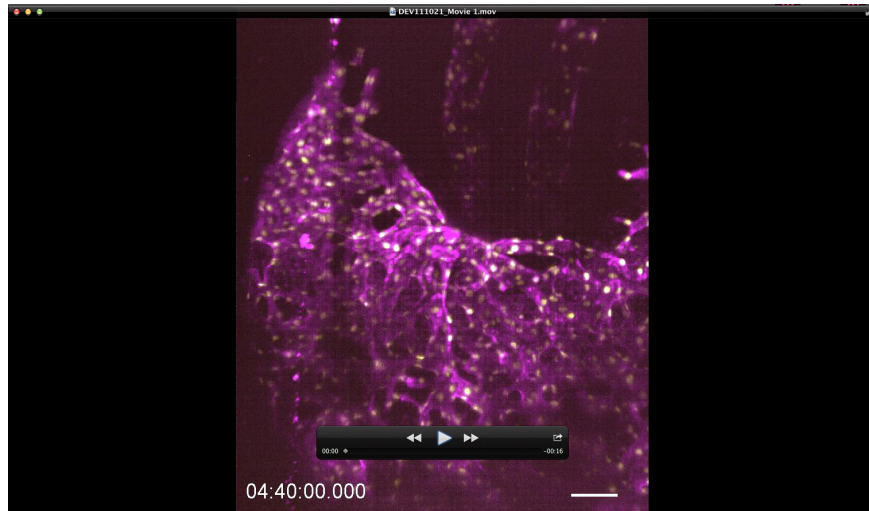
Supplementary Movie 1: Yolk sac expansion and closure. (*Flk1-myr::mCherry*; *Flk1-H2B::eYFP* vessels) showing distinct migration behaviors near the edge of the yolk sac as it closes over the embryo proper. Playback frame rate is 5 fps. Images were acquired with a 20×, NA=1.0 objective, zoom = 0.4, every 10 minutes for 16.5 h, *z*-step=2.67 μm, total *z* depth=411.18 μm. The movie shows 12 h of development from a total imaging session of 16 h. Scale bar is 100 μm.
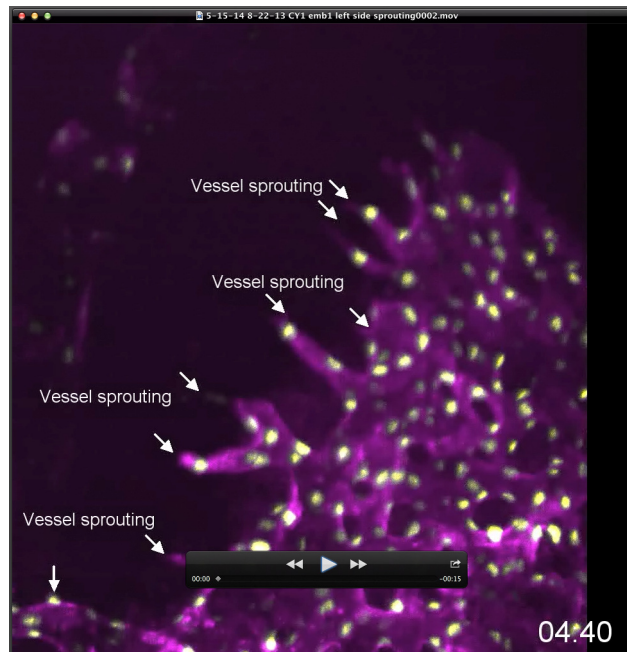
Supplementary Movie 2: Sprouting angiogenesis and anastomosis in the yolk sac at the ventral vascular/avascular border. Sprouting vessels undergo anastomosis extending the vessel bed. Playback frame rate is 3 fps. Images were acquired with a 20×, NA=1.0 objective, zoom=0.4, every 10 minutes for 7.5 h, z-step=2.67 μm, total z depth=411.18 μm.
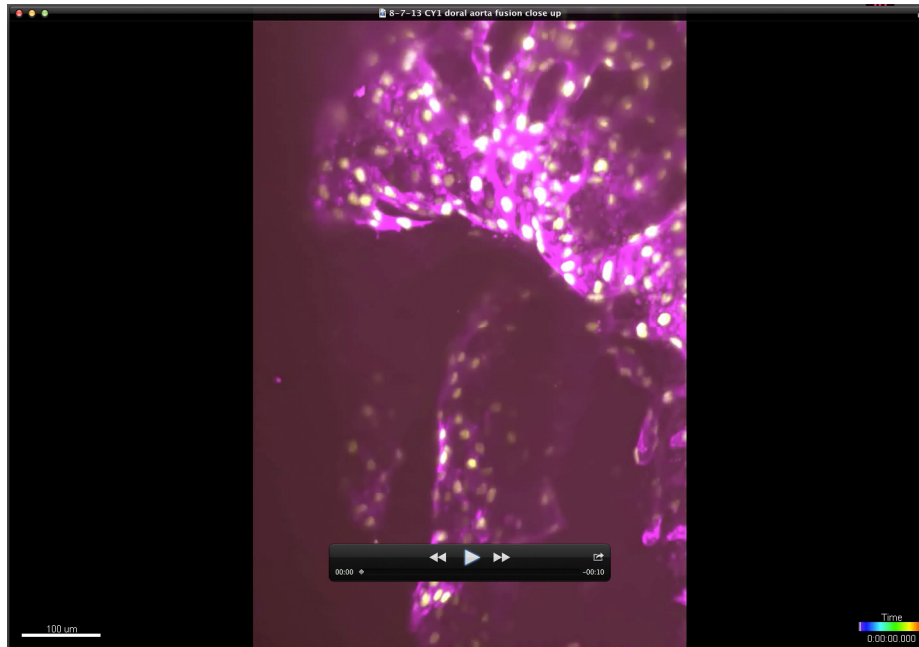
Supplementary Movie 3: Dorsal aortae fusion of *Flk1-myr::mCherry*; *Flk1-H2B::eYFP* E8.75 mouse embryo. The initial paired dorsal aortae begin as separate vessels (two large centered vessels) that fuse together (double arrows) at two separate regions along the vessel axis. Anterior is top, and posterior is bottom. Very bright, posterior *Flk1-myr::mCherry*; *Flk1-H2B::eYFP* cells are of the yolk sac vessels. Playback frame rate is 4 fps. Scale bar: 100 μm. Images were acquired with 20× objective, NA= 1.0, zoom=0.4, every 8 minutes for 7 h 36 m, *z*-step size=1.484 μm, total *z* depth=71.22 μm. Scale bar: 100 μm.
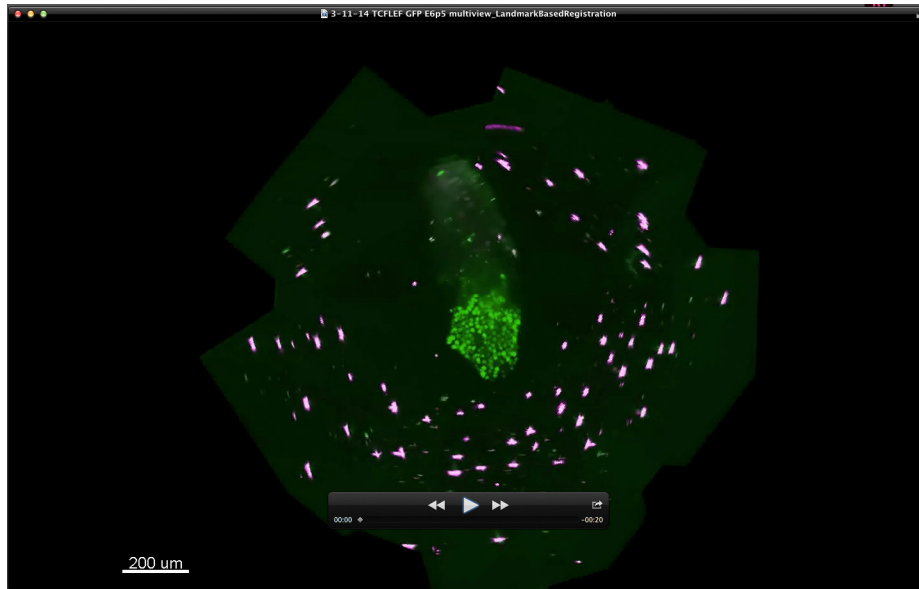
Supplementary Movie 4: 3D multiview acquired image of E6.5 *TCFLEF-H2B::eGFP* mouse embryo with red fluorescent fiducial beads embedded in the agarose cylinder (beads were also illuminated with the 488 nm laser, showing overlap of the red-green overlap of fluorescence as white). Movie starts with a posterior view, and the image rotates along the proximal (top) to distal (bottom) axis. Scale bar: 200 μm.
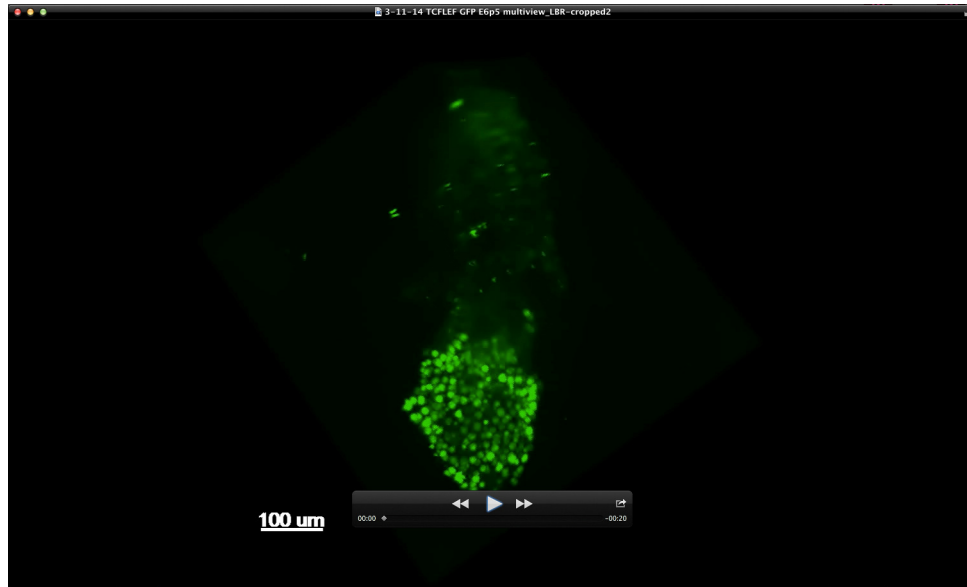
Supplementary Movie 5: Cropped 3D multiview acquired image of E6.5 *TCFLEF-H2B::eGFP* mouse embryo. Movie starts with a posterior view, and the image rotates along the proximal (top) to distal (bottom) axis. Scale bar: 100 μm.
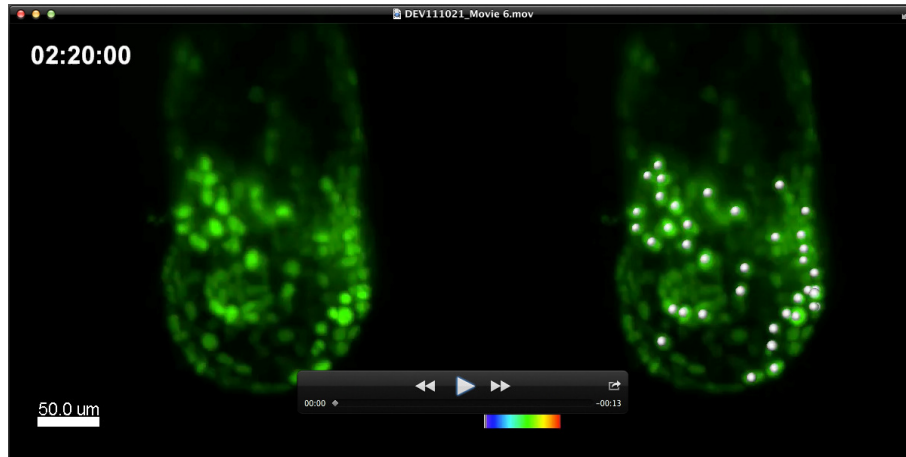
Supplementary Movie 6: Gastrulating E6.5 *TCFLEF-H2B::eGFP* mouse embryo. For all frames, the 3D time-lapse movie is on the left and the movie overlaid with 3D tracking data from Bitplane's Imaris is on the right. Embryo is oriented with anterior is to the left. Playback frame rate is 6 fps. Images were taken with a 20× objective, NA=1.0, zoom = 0.7, every 10 minutes for a total of 24 h, *z*-step size=1.14 μm, total *z* depth=115 μm. Scale bar: 50 μm.